


PAPER

Study of Stark broadening of Li i 460 and 497 nm spectral lines with independent plasma diagnostics by Thomson scattering

To cite this article: Krzysztof Dzierga *et al* 2018 *Plasma Sources Sci. Technol.* **27** 025013

View the [article online](#) for updates and enhancements.

Study of Stark broadening of Li I 460 and 497 nm spectral lines with independent plasma diagnostics by Thomson scattering

Krzysztof Dzierżęga¹ , Tomasz Pięta¹, Witold Zawadzki¹,
Evgeny Stambulchik², Marijana Gavrilović-Božović³, Sonja Jovičević³ and
Bartłomiej Pokrzywka⁴

¹ Marian Smoluchowski Institute of Physics, Jagiellonian University, ul. Łojasiewicza 11, 30-348 Kraków, Poland

² Faculty of Physics, Weizmann Institute of Science, Rehovot 7610001, Israel

³ Institute of Physics, University of Belgrade, PO Box 68, 11080 Belgrade, Serbia

⁴ Institute of Physics, Pedagogical University, ul. Podchorążych 2, 30-084 Kraków, Poland

E-mail: krzysztof.dzierzega@uj.edu.pl

Received 25 October 2017, revised 12 January 2018

Accepted for publication 29 January 2018

Published 20 February 2018



Abstract

We present results of experimental and theoretical studies of the Stark broadening of the Li I 460 nm spectral line with forbidden components and of the isolated 497 nm line. Plasma was induced by Nd:YAG laser radiation at 1064 nm with pulse duration ~ 4.5 ns. Laser-induced plasma was generated in front of the alumina pellet, with some content of Li_2CO_3 , placed in a vacuum chamber filled with argon under reduced pressure. Plasma diagnostics was performed using the laser Thomson scattering technique, free from assumptions about the plasma equilibrium state and its composition and so independently of plasma emission spectra. Spatially resolved spectra with Li lines were obtained from the measured, laterally integrated ones applying the inverse Abel transform. The Stark profiles were calculated by computer simulation method assuming a plasma in the local thermodynamic equilibrium. Calculations were performed for experimentally-inferred electron densities and temperatures, from 1.422×10^{23} to $3.55 \times 10^{22} \text{ m}^{-3}$ and from 1.96 eV to 1.04 eV, respectively. Our studies show very good agreement between experimental Stark profiles and those computer simulated.

Keywords: Stark broadening, laser-induced plasma, Thomson scattering, computer simulation technique

1. Introduction

The analysis of the Stark broadened line profiles emitted by the atoms or ions is one of the basic diagnostic methods of astrophysical, laboratory as well as industrial plasmas [1]. The shapes of these lines are very sensitive to the electric micro-fields originating from electrons and ions surrounding the emitter. That's why their main features—the width and the shift—are strongly dependent on the density of charged particles and, to a lesser extent, their kinetic temperatures. The sensitivity of line shapes to plasma micro-fields is particularly strong in the case of the linear Stark effect typical for hydrogen or hydrogen-like ions. This is a direct consequence

of the non-zero dipole moment of the hydrogen atom resulting from the degeneracy of its energy levels. The determination of the plasma electron density from the Stark broadened profiles of hydrogen lines of Balmer series, in particular H_{β} , has been a well-established and commonly used method (see e.g. [2] and references therein).

However, in the vast majority of multi-element plasmas, hydrogen lines can strongly overlap with other lines or hydrogen is not present at all. In such cases, the profiles of isolated non-hydrogenic lines are used for plasma diagnostic purposes. Compared to hydrogen lines, usually the broadening of these lines, resulting from the quadratic Stark effect, is significantly smaller. For that reason, the contribution of the

Stark broadening to the total linewidth of such lines is often more difficult to assess due to other effects (e.g., instrumental and Doppler broadening, opacity or possible Zeeman splitting) which can considerably affect the line profile [3].

An intermediate case between hydrogen and non-hydrogenic lines are the isolated lines with forbidden components ($\Delta l \neq \pm 1$, where l is an angular momentum quantum number). Such component or sometimes several components appear as a consequence of mixing of the upper or lower level of an allowed transition with a close lying perturbing level (levels) by the plasma micro-field. In other words, when the perturbation due to the plasma micro-field becomes comparable to the energy distance to the perturbing level, their wavefunctions become strongly mixed. In such circumstances the system of the emitter energy levels approaches hydrogen like (degenerate) and the linear Stark effect governs the line formation. Then, the normally forbidden line appears in the vicinity of the allowed one. These lines with forbidden components raise interest for at least two reasons. First, their shapes are very sensitive to the electron density and therefore, can be used for plasma diagnostics. Second, different Stark broadening theories can be benchmarked against the overall experimental profiles of these lines.

The most frequently studied and used lines of this type are atomic He 447.1 and 492.2 nm lines (see e.g. [4–6] and references therein). Recently, their profiles as calculated using computer simulation (CS) technique have been published for a large range of electron density n_e [7, 8]. Although the Stark broadening of He lines is relatively well researched and there are many bibliographic data, it is not always possible to use it as a plasma probe. For instance, due to high excitation energies, the population of excited states in low temperature plasma may be too low that the signal-to-noise ratio for spectral lines is insufficient to make reliable plasma diagnostics. In turn, in laser plasma induced from solid targets, the resulting shockwave prevents mixing of the plasma plume with the ambient gas which is simply not excited.

Another element, apart from hydrogen and helium, which can be considered as very sensitive plasma probe is lithium, the lightest metal with simple atomic structure, relatively abundant in the Universe. The spectral line of lithium with the highest application potential and the most frequently studied is the Li I 460.28 nm line with a forbidden component. The allowed line at 460.28 nm originates from the 4d–2p transition while the most intense forbidden component originates from the 4f–2p transition ($\Delta E_{4f-4d} = 0.84$ meV [9]). The red wing of the allowed line is slightly perturbed by another forbidden component related to the 4p–2p transition ($\Delta E_{4d-4p} = 19.07$ meV).

These lines are accompanied by the intense isolated non resonant line at 497.17 nm (4s–2p transition). This line has already been investigated experimentally but only in few publications the values of its Stark widths and shifts were reported together with accurate plasma parameters [10, 11]. The overall profiles of this isolated line were calculated by Benett and Griem (BG) [1, 12] and by Dimitrijević *et al* (DSB) [13–15] and are presented in the form of tables. Within the BG approach, interactions of radiating atom with electrons

and ions are calculated using the impact and quasi-static approximation, respectively. On the other hand, DSB provides only reliable electronic contribution to the Stark width since the influence of ions is considered within the impact approximation which breaks for moderate and high n_e .

For the first time, the Li I 460 nm line was investigated by Grechikhin and Tyunina [16] in dc arc at low $n_e \sim 10^{21} \text{ m}^{-3}$. In fact, electron densities were inferred by comparing the measured line profiles with calculations performed by Sassi [17] for n_e in the range of $(0.1\text{--}1.5) \times 10^{22} \text{ m}^{-3}$. Much more comprehensive studies, experimental and theoretical, have been recently performed by Cvejić *et al* [18]. The overall line shapes, measured in laser-induced plasma (LIP), were compared with those calculated by the CS method. Once again, plasma diagnostics was made with the use of the other line profile—the Li isolated one 497.17 nm. For n_e evaluation, its shape as computed either with CS or BG method, was superimposed on the measured one while the plasma temperature was determined from relative Li lines intensities using the Boltzmann plot technique.

Obviously, in order to exploit the Li lines for plasma diagnostics, including the line with the forbidden component, reliable verification of the results of the calculation becomes indispensable.

The aim of this work is detail investigations of the Stark profiles of Li lines, the isolated one and with the forbidden component, in order to verify the results of their numerical calculations by the CS method. To this end, plasma induced by laser ablation (LIP) of solid samples containing lithium admixtures was used. The advantage of LIP, with respect to other plasma sources, is the ability to excite any element, the high repeatability, and above all the wide range of electron concentrations that occur at the subsequent stages of plasma evolution. The analysis of temporally and spatially resolved emission spectra includes effects of self-absorption as well as Doppler and instrumental broadening.

Any investigation of the spectral line profiles, resulting from the emitter—medium interaction, requires the knowledge of the physical properties of this medium which is of paramount importance. In the present study, for LIP diagnostics we used a method completely independent of plasma emission spectra, namely the laser Thomson scattering (TS) [19]. Principal advantages of TS are high spatial and temporal resolutions and ease with which the measured data can be interpreted. The standard plasma parameters—the electron temperature and density—can be directly derived from the electron feature of the TS spectrum. Moreover, unlike e.g. optical emission spectroscopy, the results do not depend on assumptions of the plasma thermodynamic equilibrium, its chemical composition or a selected theoretical model used in the line profile calculations. Finally, in this work, calculations of Stark profiles for both investigated lines were performed within the same model using an implementation of the CS method [20]. Importantly, the calculations were performed exactly for LIP parameters determined by TS method.

The presented approach, i.e., the combination of accurate calculations, high-quality line profile measurements and

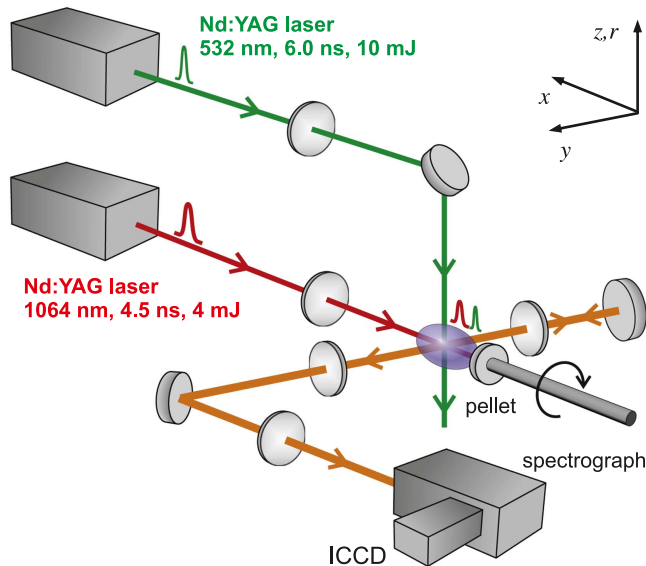


Figure 1. Scheme of the experimental setup.

independent plasma diagnostics, is unique and allows for a very reliable validation of the theoretical model describing so different systems with non-degenerate as well as nearly degenerate energy levels.

2. Experiment

The scheme of the experimental setup is depicted in figure 1. A vacuum chamber was evacuated below 0.1 mbar and then purged with argon at 200 mbar at a constant flow rate of 30 l h^{-1} . Plasma was generated by a Q-switched Nd:YAG laser (1064 nm, 3.5 mJ), operating at a repetition rate of 10 Hz, with a pulse duration of $\sim 4.5 \text{ ns}$. The laser beam was focused about 1 mm behind the front surface of the continuously rotated target sample, to the spot of about $100 \mu\text{m}$ in diameter at the surface. The target were alumina Al_2O_3 : Li_2CO_3 : MgCO_3 (9:4:1) pellets. All experimental parameters were matched to have shot to shot highly reproducible plasma plume. For the laser TS, a separate, single mode ($\delta\lambda < 0.28 \text{ pm}$), Nd:YAG laser with $\sim 6.0 \text{ ns}$ pulse duration at 532 nm (the second harmonic) was used. This laser beam was propagating orthogonally to the first, plasma generating one, and was polarized perpendicularly to the observation direction. The beam was collimated to the spot of about $200 \mu\text{m}$ in diameter in the plasma volume and pulses of 10 mJ energy were applied. The delay between pulses of two lasers was controlled by a digital delay pulse generator with accuracy better than 0.5 ns. The emission from LIP and the laser-scattering light were observed in a direction perpendicular to the plane of laser beams by imaging the investigated plasma plume onto the entrance slit of a Czerny-Turner spectrograph (750 mm focal length, 1.005 nm mm^{-1} reciprocal dispersion) with 1.2 magnification. Plasma imaging was performed using the zeroth order of the spectrograph with the entrance slit fully open. Imaging allowed verification of the plasma reproducibility, its positioning with respect to the

probe laser beam as well as selection of a specific plasma layer for further investigations. The spectra of the scattered light and the LIP emission were recorded over a wavelength range of 13.3 nm with slit widths of $50 \mu\text{m}$ and $30 \mu\text{m}$, respectively. The instrumental profile for the emission part of the experiment was measured using a low pressure Hg spectral lamp and is well described by the gaussian function with 0.045 nm FWHM. Self absorption of studied Li I spectral lines was verified with the back-reflecting mirror method as described in Cvejić *et al* [21]. The spectral sensitivity of the experimental system was corrected for, using a halogen-deuterium lamp. In order to probe the specific layer of the plasma plume, the laser beam focusing lens and the pellet holder were mounted on two separate translation stages which were moved by the same distance to maintain laser fluence on the surface of the sample.

The optical signals were collected using a gated two dimensional intensified charge-coupled device (ICCD) camera synchronized to the probe and plasma-generating pulses in case of TS and emission measurements, respectively. In order to improve the signal-to-noise ratio of TS spectra, the ICCD gate width was as short as 6 ns. On the other hand, emission signals were recorded at gate widths set to 3% of the respective delay time, e.g., 18 ns for 600 ns delay. This way, the decrease in electron density during emission measurements was below 3% and the plasma could be treated as quasi stationary. Laser-scattering and emission spectra were averaged, respectively, over 2000 and 5000 laser shots and were investigated in the time interval from 600 to 2200 ns after plasma-generating laser pulse and from plasma layers 0.6 to 0.8 mm from the target surface. In case of TS measurements, a razor edge filter was placed in front of the spectrograph, to block radiation below 533.0 nm, protecting the ICCD from saturation by strong stray laser light scattered off the sample surface and its holder.

3. Experimental results

3.1. Plasma diagnostics by laser TS method

Selected plasma images as well as spatially resolved TS and emission spectra, determined at different instants after the ablating laser pulse, are shown in figure 2. The long-wavelength part of TS spectra (with subtracted plasma background) reveals distinct maximum indicating partially collective character of the TS process. Hence, fitting the spectral density function to the experimental data yields both the electron density and the electron temperature without having to calibrate the power of the scattered light [19, 22]. Typical fits are presented in figure 3. It should be clearly stated that the fitted model is free from assumptions about the thermodynamic equilibrium and the chemical composition of the plasma. Radially resolved n_e and T_e are presented in figure 4. Their distributions are homogeneous in the great part of the plasma column and expand with time. The unusual increase of the electron temperature at the edge ($|r| \gtrsim 0.5 \text{ mm}$) of the plasma can be explained (to some extent) by the

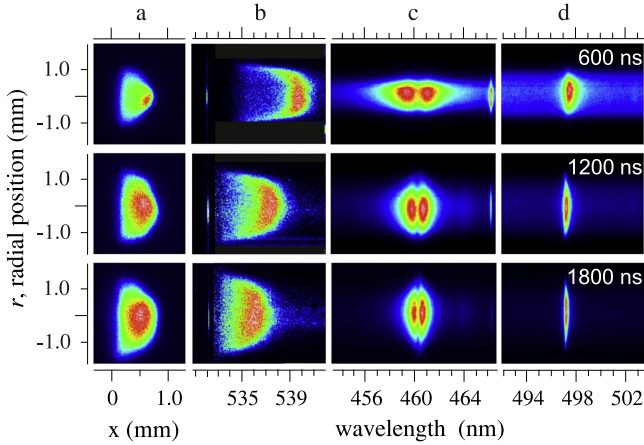


Figure 2. Experimental results for lithium LIP. Plasma images (a) with the origin at the target surface. Radial distribution of the electron feature of the laser Thomson scattering spectrum (b) after subtraction of plasma emission background while illuminating plasma layer 0.6 mm (600, 1200 ns) or 0.8 mm (1800 ns) away from the sample surface. The signal at 532 nm corresponds to the probe laser due to the finite absorption of the razor edge filter and is the absolute reference for the wavelength scale. Lateral distributions of Li I 460 nm (c) and Li I 497 nm (d) spectral lines' intensities for the same LIP layers as in (b).

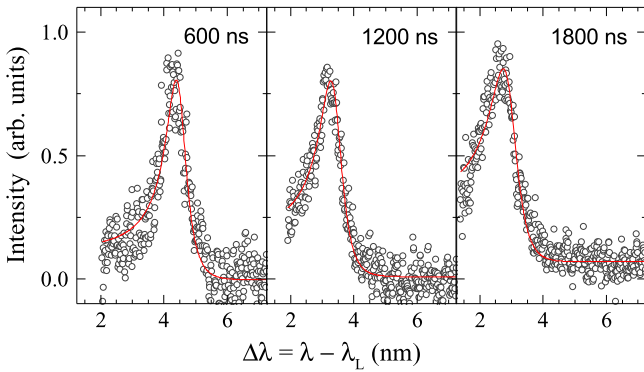


Figure 3. Experimental TS spectra (empty circles) collected from the central part of the plasma column fitted with the spectral density function (red lines).

limited spatial resolution of our experimental system determined by the size of the probe laser beam. A rapid decrease in n_e in these areas, at distances smaller than the resolving power, results in decrease of the plasma frequency and a subsequent shift of the TS spectrum of a collective or partially-collective character. As a result, such rapid changes in the TS spectra in space lead to the broadening of the recorded spectrum and ultimately result in elevated value of the fitted T_e . Similar changes in n_e in the case of non-collective TS have little effect on the calculated electron temperature. For further studies only central, homogeneous plasma core with a radius of about 0.2 mm, was considered. This way the influence of short-time plasma instabilities and spatial inhomogeneities on final results is greatly reduced. The temporally resolved n_e and T_e on the plasma axis are presented in figure 5. The electron density decreases from $1.422 \times 10^{23} \text{ m}^{-3}$ at 600 ns to $0.355 \times 10^{23} \text{ m}^{-3}$ at 2200 ns after the ablating laser

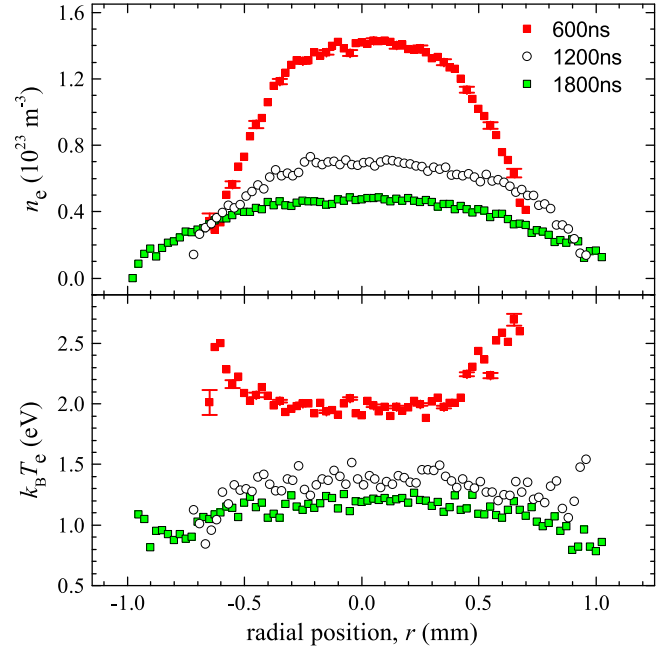


Figure 4. Radial (across the plasma plume) distribution of electron density and temperature determined at various moments after the laser pulse generating the plasma.

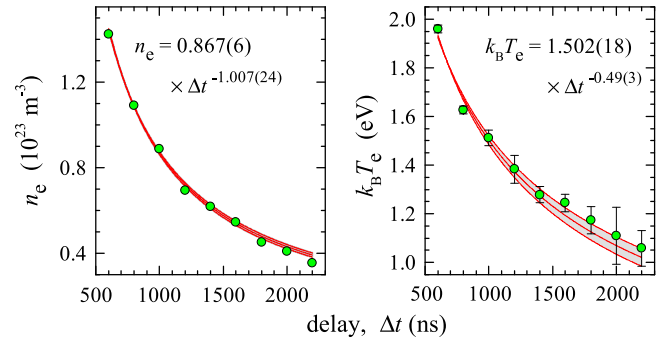


Figure 5. Temporal evolution of electron density and temperature on the plasma axis fitted with power laws.

pulse. At the same time, the measured electron temperature drops from about 1.96 to 1.04 eV.

The uncertainties of n_e and T_e were evaluated based on statistical uncertainties of the fitted spectral density function to the experimental TS spectrum and also taking into account their scattering in the central plasma region. The uncertainty of the electron temperature can be enlarged due to possible electron heating by the probe laser pulse in the inverse bremsstrahlung process. This effect was carefully verified by measurements at different energies of the probe pulse and it was recognized as negligible under our experimental conditions. Additional uncertainties in determining plasma parameters, important for Stark profile studies, are due to different time accumulations of TS and emission spectra on the ICCD. Namely, while TS spectra were recorded over 6 ns independently of the delay, accumulation time of emission spectra was increasing from 18 ns to 66 ns at delays of 600 ns and 2200 ns, respectively. Systematic uncertainty related to such *gate width effect* was determined by first fitting the power

Table 1. Plasma parameters and characteristics of the Li I 460 nm line profiles as determined at various moments of plasma evolution. FWHM, F/A and $\Delta\lambda_{af}$ stand for the full width at half maximum, the intensity ratio of the forbidden to the allowed component and the separation between allowed and forbidden peaks, respectively. Exp—experimental data, CS—computer simulation method.

Delay (ns)	n_e (10^{23} m^{-3})	$k_B T_e$ (eV)	FWHM (nm)		F/A		$\Delta\lambda_{af}$ (nm)	
			Exp	CS	Exp	CS	Exp	CS
600	$1.422^{+0.012}_{-0.054}$	$1.96^{+0.02}_{-0.07}$	4.57 ± 0.11	4.43 ± 0.18	1.031 ± 0.021	1.008	1.806 ± 0.011	1.741
800	$1.091^{+0.004}_{-0.036}$	$1.63^{+0.02}_{-0.07}$	3.68 ± 0.11	3.56 ± 0.14	0.978 ± 0.029	0.978	1.468 ± 0.009	1.473
1000	$0.886^{+0.016}_{-0.041}$	$1.51^{+0.03}_{-0.08}$	3.11 ± 0.07	3.08 ± 0.12	0.980 ± 0.021	0.969	1.212 ± 0.008	1.273
1200	$0.694^{+0.022}_{-0.043}$	$1.38^{+0.06}_{-0.10}$	2.63 ± 0.04	2.60 ± 0.11	0.971 ± 0.037	0.937	1.056 ± 0.006	1.112
1400	$0.618^{+0.011}_{-0.029}$	$1.28^{+0.03}_{-0.07}$	2.38 ± 0.04	2.39 ± 0.10	0.944 ± 0.040	0.931	0.968 ± 0.008	0.964
1800	$0.452^{+0.015}_{-0.029}$	$1.20^{+0.06}_{-0.09}$	1.89 ± 0.04	1.93 ± 0.08	0.911 ± 0.020	0.892	0.760 ± 0.004	0.790
2200	$0.355^{+0.015}_{-0.026}$	$1.04^{+0.07}_{-0.10}$	1.55 ± 0.03	1.61 ± 0.06	0.882 ± 0.016	0.871	0.638 ± 0.003	0.683

laws to decays of n_e and T_e with time (see figure 5) and then evaluating their decrease over the time period equal to the applied gate. The final—statistical plus systematic—uncertainties for plasma parameters are presented in tables 1 and 2.

3.2. Determination of Stark parameters of Li I 497 and 460 nm spectral lines

Figures 2(c) and (d) show images of laterally integrated emission spectra of LIP, observed in the spectral range of the investigated Li I lines and at plasma conditions as for TS experiment. These original data were first corrected for dark current of the ICCD, smoothed using the Savitzky–Golay filtering and then they were corrected for the self absorption effect if needed. Such procedure allows to treat the resulting profiles as originating from the optically thin medium in further analysis. Radially resolved spectra were then obtained applying the inverse Abel transform in the same way as it has been recently described by Cvejić *et al* [18, 21]. In further analysis, only the spectra obtained for the central, homogeneous part of the plasma column (see figure 4), i.e. within a radius of 0.2 mm, were considered.

The resulting spectra contain the corresponding atomic lithium line but also continuous plasma radiation which was assumed to be constant for each of the studied lines.

The 460 nm line profile was obtained by subtracting the signal of continuous radiation which was assumed to be equal to the signal at the distant blue wing of that line. In this case, the signal at the red wing was not considered due to its disturbance by the 466.3 nm ionic aluminum line. Such profiles obtained for the plasma axis ($r = 0.0$ mm) and for various delays are shown in figure 6. The position and intensity of each single peak (allowed and forbidden) was determined by fitting to each of them a Lorentz function in a narrow spectral range. On this basis, the parameters of the line profile such as FWHM, the the intensity ratio F/A of forbidden to allowed component and their separation $\Delta\lambda_{af}$ were calculated and are listed in table 1.

Determining the Stark profile of the 497 nm line requires much more precise data processing than for the 460 nm line. This is due to its much smaller width as well as its asymmetry, mainly caused by the ion broadening. Therefore, spectra were first approximated by two Lorentz/Voigt

profiles on a constant plasma background. This background was then subtracted from these experimental spectra and final line profiles were obtained as shown in figure 7. Then, the apparatus function and the Doppler broadening (FWHM = 0.021 nm at $k_B T_e = 1.04$ eV) were removed by numerical deconvolution using an iterative method proposed by Drawin [23]. Finally, the line parameters—FWHM, the asymmetry defined as $\text{HWHM}_{\text{red}}/\text{HWHM}_{\text{blue}}$ and the line shift—were determined and they are presented in table 2. The line shift was calculated relative to the line position observed on the plasma edge.

The uncertainties of these line parameters are evaluated based on statistical uncertainties of the fitted parameters and the law of error propagation. The largest uncertainty comes from the line position and has a significant effect, predominantly on the accuracy of the asymmetry of the line profile.

4. CSs of line profiles

CS methods for spectral lineshape modeling [24] have been in increasing use for a few decades since the pioneering work of [25]. Through the calculations, motion of a statistically representative number of perturbers is modeled. The resulting electric-field histories, as seen by the radiators, are used to obtain time evolution of the latter, allowing for obtaining the radiation spectrum. Such calculations are generally believed to be the most reliable type of Stark broadening models [26] as long as the very few approximations assumed are satisfied. Among these approximations the most important one is the classical motion of the perturbers, in particular, electrons. The accuracy of the calculations will be discussed below.

For the calculations presented in this study, an implementation of CS lineshape modeling was used [20]. Here, motion of Debye quasiparticles is, in general, obtained by accounting for monopole interactions between them and the radiator, placed at the center of a simulation sphere, using a velocity Verlet algorithm [27]. However, for the present calculations, the radiators are neutral, therefore, the trajectories of all plasma particles were assumed straight. The screening length λ_s of particles of species s is calculated in the

Table 2. Plasma parameters and characteristics of the Li I 497 nm line profiles as determined at different instants of plasma evolution. FWHM stands for the full width at half maximum and the asymmetry of the profile is defined as the ratio of the red to the blue HWHM. Exp—experimental data, CS—computer simulation method, BG—Benett and Griem [1], DSB—Dimitrijević and Sahal-Bréchet [14].

Delay (ns)	n_e (10^{23} m^{-3})	$k_B T_e$ (eV)	FWHM (nm)				$\Delta\lambda$ (nm)				Asymmetry		
			Exp	CS	BG	DSB	Exp	CS	BG	DSB	Exp	CS	BG
600	$1.422^{+0.012}_{-0.054}$	$1.96^{+0.02}_{-0.07}$	0.853 ± 0.030	0.939 ± 0.056	1.110	0.799	0.486	0.457	0.525	0.561	1.39 ± 0.07	1.125	1.181
800	$1.091^{+0.004}_{-0.036}$	$1.63^{+0.02}_{-0.07}$	0.626 ± 0.030	0.682 ± 0.041	0.822	0.603	0.317	0.349	0.400	0.429	1.43 ± 0.08	1.128	1.178
1000	$0.886^{+0.016}_{-0.041}$	$1.51^{+0.03}_{-0.08}$	—	0.540 ± 0.032	0.651	0.484	—	0.282	0.323	0.348	—	1.110	1.164
1200	$0.694^{+0.022}_{-0.043}$	$1.38^{+0.06}_{-0.10}$	0.391 ± 0.020	0.413 ± 0.025	0.497	0.375	0.220	0.220	0.251	0.271	1.14 ± 0.03	1.171	1.156
1400	$0.618^{+0.011}_{-0.029}$	$1.28^{+0.03}_{-0.07}$	0.321 ± 0.010	0.358 ± 0.021	0.438	0.332	0.188	0.193	0.223	0.241	1.21 ± 0.04	1.122	1.152
1800	$0.452^{+0.015}_{-0.029}$	$1.20^{+0.06}_{-0.09}$	0.238 ± 0.005	0.262 ± 0.016	0.311	0.240	0.140	0.156	0.162	0.175	1.20 ± 0.03	1.093	1.143
2200	$0.355^{+0.015}_{-0.026}$	$1.04^{+0.07}_{-0.10}$	0.188 ± 0.003	0.195 ± 0.012	0.239	0.187	0.116	0.112	0.126	0.136	1.04 ± 0.01	1.104	1.104

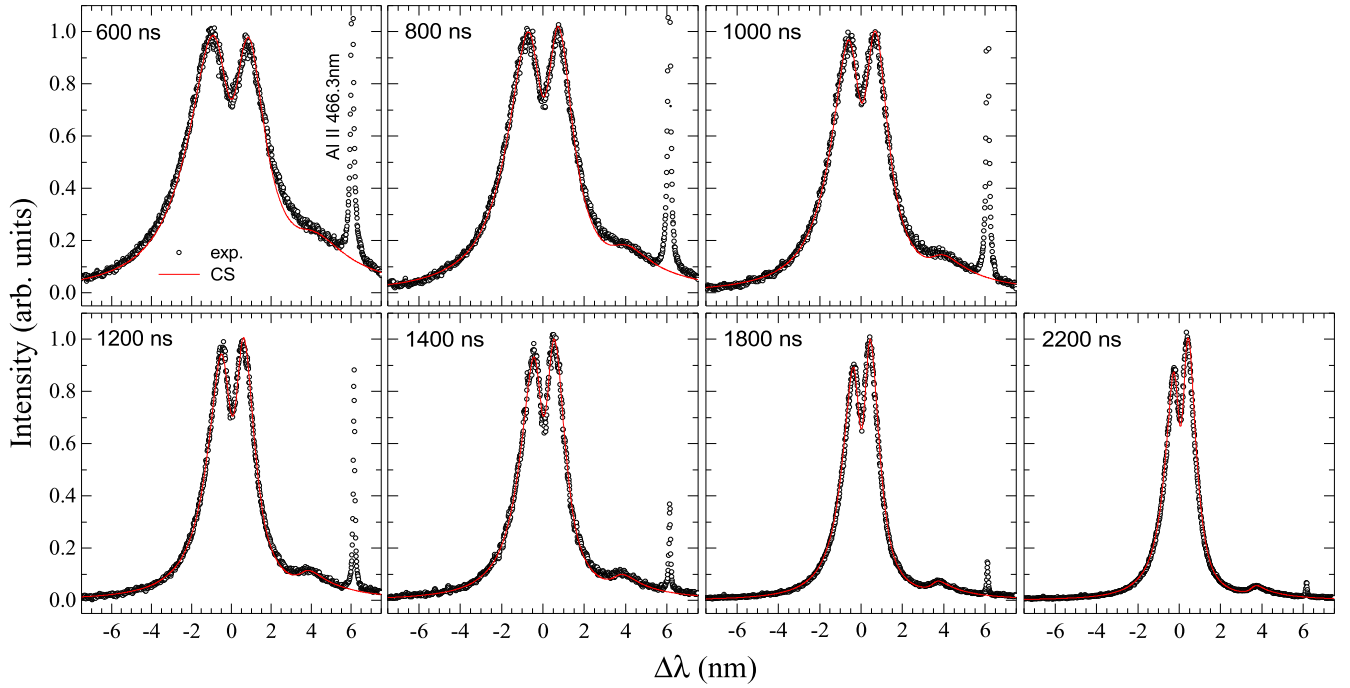


Figure 6. Experimental (empty circles) and theoretical (red lines) Stark profiles of the Li I 460 m spectral line. Calculations performed using CS method for n_e and T_e independently determined by the laser Thomson scattering method. The zero wavelength corresponds to the position of the unperturbed 2p–4d transition.

assumption that a given particle is screened by all other types of particles not exceeding it by mass:

$$\lambda_s = \left(\sum_{m_{s'} \leq m_s} \frac{4\pi n_{s'} e^2 Z_{s'}^2}{k T_{s'}} \right)^{-1/2}, \quad (1)$$

where $m_{s'}$, $n_{s'}$, $Z_{s'}$, and $T_{s'}$ are, respectively, the mass, the density, the charge, and the temperature of species s' . The Debye potential is used to calculate the electric field acting on the radiator. The radius of the simulation volume, a is always a few times the largest Debye length (which is the electron Debye length λ_e), i.e., $a \gg \lambda_e$. Such very fast simplified Debye-quasiparticle molecular dynamics simulations provide rather accurate results for weakly-to-moderately coupled plasmas, as follows from comparisons with fully-interacting- N -body simulations [28, 29]. For each pair of electron density and temperature, the plasma composition was calculated assuming that local thermodynamic equilibrium exists in LIP, as described in [18].

The Hamiltonian of the atomic system of the radiator is the sum of the unperturbed Hamiltonian H_0 and a time-dependent perturbation V :

$$H = H_0 + V(t), \quad (2)$$

where the perturbation is due to the simulated plasma electric field \vec{F} acting on the dipole moment \vec{D} of the radiator:

$$V = -\vec{F} \cdot \vec{D}. \quad (3)$$

The time-dependent Schrödinger equation is numerically solved by introducing the time-development operator $U(t)$ in the interaction representation:

$$i\partial U(t)/\partial t = V(t)U(t). \quad (4)$$

(here and below, $\hbar = 1$ is assumed). The time evolution of the dipole operator $D(t)$ is then obtained:

$$D(t) = U(t)^\dagger D U(t), \quad (5)$$

and its Fourier transform (FT),

$$\vec{D}(\omega) = \int_0^\infty dt \exp(-i\omega t) \vec{D}(t), \quad (6)$$

is used to calculate the line spectrum in the dipole approximation:

$$I(\omega) \propto \frac{1}{2\pi} \sum_{i,f} \omega_{fi}^4 |\langle \vec{D}_{fi}(\omega) \rangle|^2. \quad (7)$$

Here, the i and f indices run over the initial and final levels, respectively, $\omega_{fi} = E_i - E_f$ is the level-energy difference, and the angle brackets denote an averaging over several runs of the code (which corresponds to an averaging over a statistically-representative ensemble of radiators).

For lineshape calculations of both 460 and 497 nm lines, the Hamiltonian contained all states with the principal quantum number n from 2 to 5. The coupling between states with different n 's was important for obtaining accurate line shapes. In the case of the 460 nm line, these $\Delta n \neq 0$ couplings were crucial for reproducing the asymmetry of the peak intensities. This is demonstrated in figure 8, where the Stark-mixed and broadened spectra of the 2p–4d, 2p–4p, and 2p–4f (the latter two are dipole-forbidden in the absence of the plasma microfields) transitions are shown. The calculations were done for the TS-inferred plasma parameters corresponding to the time delay of 600 ns. From the figure it is seen that for the rather high density assumed for the calculations, the inclusion of the $n = 3$ and $n = 5$ states actually inverses

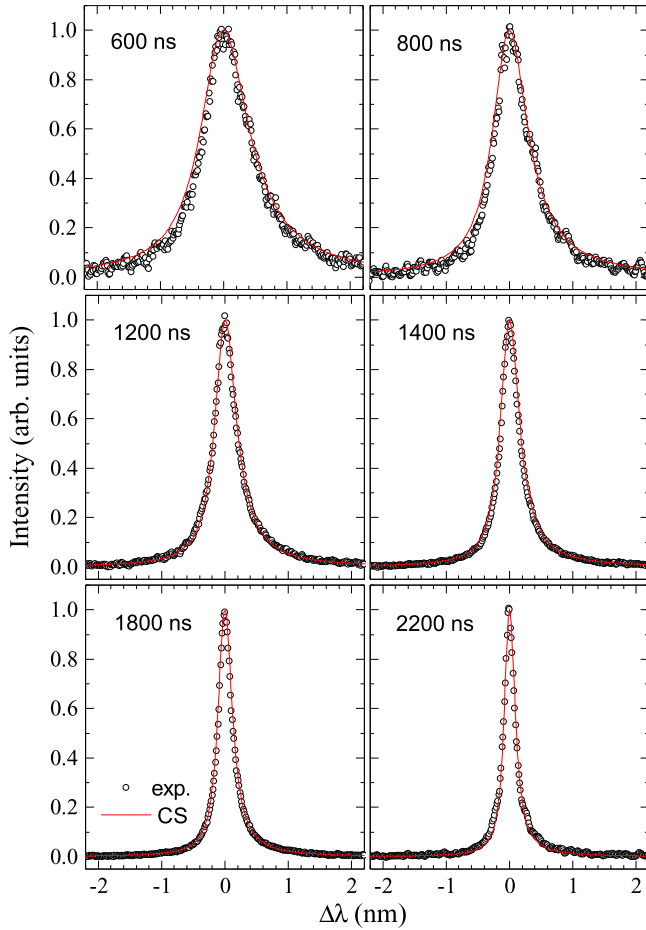


Figure 7. Experimental (empty circles) and theoretical (red lines) Stark profiles of the Li I 497 nm spectral line. Calculations performed using a computer simulation method for n_e and T_e independently determined by the laser Thomson scattering method. The zero wavelength corresponds to the position of the unperturbed 2p–4s transition.

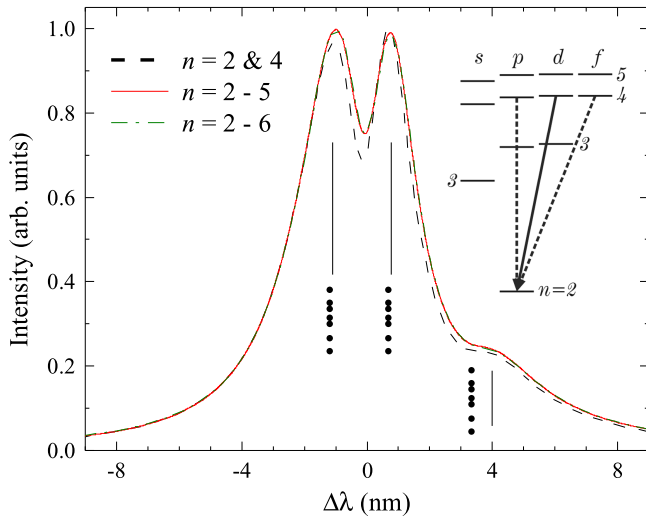


Figure 8. CS Stark profiles of the Li I 460 nm line, calculated for $n_e = 1.42 \times 10^{17} \text{ cm}^{-3}$ and $k_B T_e = 1.96 \text{ eV}$ using different Hamiltonian bases. The zero wavelength corresponds to the position of the unperturbed, dipole-allowed 2p–4d transition. For the sake of comparison, all lineshapes are peak-normalized to unity.

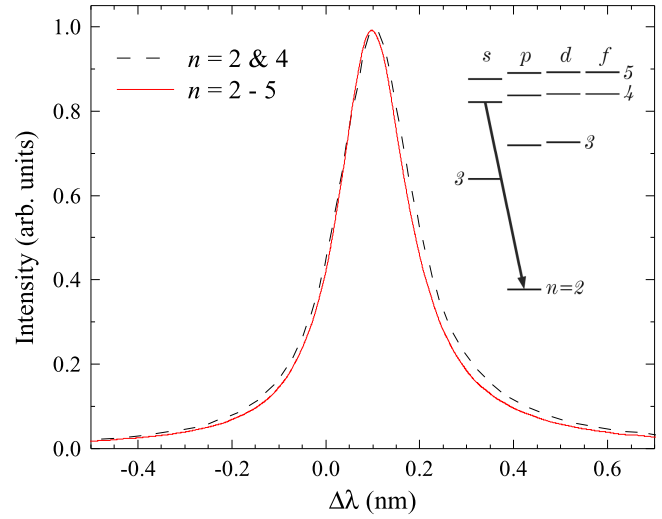


Figure 9. CS Stark profiles of the Li I 497 nm line, calculated for $n_e = 3.55 \times 10^{16} \text{ cm}^{-3}$ and $k_B T_e = 1.04 \text{ eV}$ using different Hamiltonian bases. The zero wavelength corresponds to the position of the unperturbed 2p–4s transition. The lineshapes are peak-normalized to unity.

the asymmetry (i.e., the intensity ratio of the two main peaks) of the total lineshape—in addition to a minor increase of the linewidth. However, inclusion of higher, $n = 6$ states produced no visible changes, as is evident from the figure.

Remarkably, for the 497 nm line the effect of inclusion of the $\Delta n \neq 0$ couplings is a minor but noticeable *narrowing* of the line, as well as a similar decrease of the line shift. This is shown in figure 9 for the TS-inferred plasma parameters corresponding to the time delay of 2200 ns. The narrowing of the line with inclusion of additional states is a clear indication of importance of elastic collisions for the Stark broadening of this line. The elastic contribution to broadening of an isolated line results from a *difference* of the forward-scattering amplitudes off the initial and final levels [30], and this difference may be decreased due to unequal contributions of other levels to the scattering amplitudes of the initial and final states, not unlike a strong cancellation of the static Stark shifts due to high- n states [31].

As was mentioned above, the most important assumption of the CS lineshape modeling is the classical motion of the perturbers, in particular, electrons, including neglect of the ‘back reaction’ from the radiator to the perturber [24] in the course of an inelastic collision. The relevant criterion is $|1 - \exp(-\Delta E/k_B T_e)| \ll 1$, where k_B is the Boltzmann constant and ΔE is the energy separation between Stark-interacting states. For degenerate or nearly-degenerate atomic systems such as hydrogen-like atoms or Rydberg states, this condition is usually satisfied. This is also true for the Li I 460 nm line, the Stark broadening of which is largely determined by the 4d–4f dipole interaction, with the two levels separated by only $\approx 0.6 \text{ meV}$ [32], orders of magnitude smaller than the electron temperatures inferred in the present study, $k_B T_e \sim 1\text{--}2 \text{ eV}$. Therefore, for the plasma conditions typical for the current study, the Stark broadening of this line is described by the semiclassical CS model very accurately.

The Li I 497 nm line, on the other hand, has the main broadening contribution due to the 4s–4p dipole interaction, with the respective energy separation $\Delta E_{4s-4p} \approx 0.18$ eV [9]. This implies an uncertainty of 10%–15% for the inelastic broadening. However, the inelastic broadening usually constitutes a minor part of the total Stark broadening of isolated lines of neutral species at low energies of perturbers [1]. The aforementioned decrease of the total Stark broadening due to the $\Delta n \neq 0$ contributions confirms this. Therefore, we believe that the associated inaccuracy is $\lesssim 5\%$ for this line.

In order to check for possible influence of higher-than-dipole moments of the plasma–radiator interaction, calculations for a few selected values of the plasma density and temperature were performed accounting for the quadrupole terms, i.e., with equation (3) becoming

$$V = -\vec{F} \cdot \vec{D} - \frac{1}{6} \sum_{ij} \frac{dF_i}{dx_j} Q_{ij}, \quad (8)$$

where Q is the quadrupole tensor of the radiator, with its matrix elements calculated using the R W Cowan's code [33]. However, this extension resulted in negligible changes of the shapes of both lines ($\lesssim 1\%$ difference of FWHM). This is in agreement with another study [34] of a similar atomic system (hydrogen Balmer- β line, which is also an $n = 4$ to $n = 2$ transition), where the quadrupole and higher multipole plasma–radiator interactions resulted in a $\sim 5\%$ linewidth increase at an order-of-magnitude higher density.

Each lineshape was averaged over 1000–2000 runs, corresponding to a statistical uncertainty of 2%–3%. This was checked by a convergence analysis as described in [35].

To summarize, the total theoretical uncertainties (one standard deviation) are estimated to be within 4% and 6% for the width of the 460 nm and 497 nm lines, respectively. The relative uncertainties of the shift calculations of the 497 nm line are likely to be larger, $\sim 10\%$ due to the cancellation effects [31].

In practice, the FT in equation (6) is a discrete FT over a finite time t_{\max} . This introduces an extra numerical extension of the profile $\approx c/t_{\max}$ (in the wavenumber units; c is the speed of light), approximately of the Lorentzian form. For the 460 nm line, the respective broadening was about 1%–2% of the line FWHM, well below the estimated inaccuracy. However, in the case of the much narrower 497 nm transition, especially at lower electron densities (e.g., as shown in figure 9), it reached 6%–8%. Therefore, this extra linewidth was subtracted from the calculated 497 nm profiles by performing deconvolution of the respective Lorentzians using again an iterative method proposed by Drawin [23] with an improvement dependent on the spline interpolation between grid points. The final line profile parameters calculated by CS method at the TS-inferred plasma conditions are presented in tables 1 and 2.

After corrections for such numerical broadening, the CS calculated lineshapes were convoluted with the instrumental and Doppler-broadening functions for comparison with the experimental profiles and are shown in figures 6 and 7.

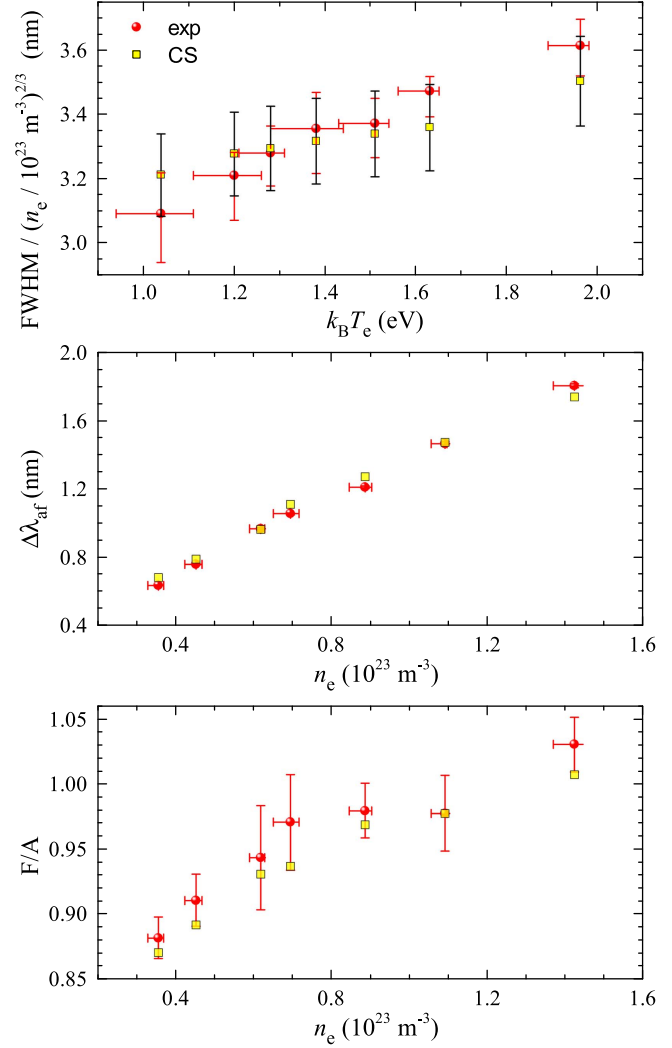


Figure 10. FWHM of the Li I 460 nm spectral line normalized to $n_e^{2/3}$, the amplitude ratio F/A of the forbidden (2p–4f) to the allowed (2p–4d) component and their separation $\Delta\lambda_{af}$.

5. Discussion

5.1. The Li I 460 nm line profile

The 460 nm line profiles containing allowed and forbidden components, both those experimentally determined and those computer simulated, are shown in figure 6. Their characteristics—FWHM, the amplitude ratio F/A and separation between the forbidden and allowed peaks—depending on plasma parameters as obtained by the TS method—are presented in figure 10 and collected in table 1.

Despite the tremendous application potential of this line in plasma diagnostics, there are virtually no other data, either experimental or theoretical, with which we could directly compare the results of our investigations. Calculations concern only the allowed component [14, 17, 36] and only the work [14] covers the range of plasma parameters studied in this work. On the other hand, the experimental data were mainly obtained for plasmas with significantly lower electron concentrations and temperatures. Also previous work [18]

concerned plasma with significantly lower electron temperature $k_B T_e \sim 0.35 \div 0.6$ eV.

As it is evident, the experimental results and calculations are consistent within the uncertainty limits, with a maximum deviation of 4% for FWHM and F/A and 7% for $\Delta\lambda_{af}$. Discrepancies exist mostly for the red wing of the line profile (see figure 6) that grow with electron concentration and temperature. These discrepancies may partly result from assuming isothermal plasma. However, detailed studies on LIPs [37, 38] show that it is very likely that in such circumstances the electron temperature greatly exceeds the kinetic temperature of the heavy particles. Moreover, in analysis of the plasma spectrum, it was assumed that the line under study is not overlapping. In fact, there are several spectral lines originating from highly excited states of the ionic aluminum. Their significance increases with electron concentration and temperature. These lines are indistinguishable from the line of interest and increase our uncertainties to an extent difficult to estimate.

5.2. The Li I 497 nm line profile

The 497 nm full line profiles, the experimentally determined and computer simulated for the TS-inferred n_e and T_e , are presented in figure 7. In turn, their characteristics such as FWHM, the asymmetry and the line shift are collected in table 2 and they are also shown in figure 11. For the sake of comparison, in the same table and figure, the results of calculations carried out using the semiclassical approach by BG [1, 12] and by DSB [13–15] are also presented. Because DSB model only provides the electron impact linewidth and shift, therefore the ion broadening parameter A , as calculated within BG model, was used to infer the total Stark widths and shifts of the studied line.

As can be observed, the FWHM obtained with CS and BG methods are larger than those measured in this work while the DSB gives slightly narrower profiles. CS profiles are about 9% broader than experimental ones but it is still within uncertainty limits considering the lower and upper error bars of n_e . This discrepancy can not be attributed to self absorption because the effect would be reversed, i.e. the experimental profile would be broader. In the case of the line shifts, the measured values are about 15% and 20% smaller than those calculated from the BG and DSB models, respectively. At the same time, there is very good compatibility with the CS calculations just like for $\Delta\lambda_{af}$ of the Li I 460 nm line.

Stark parameters, although to a lesser extent, are also temperature dependent. Figure 11 shows the normalized (to $n_e = 10^{23} \text{ m}^{-3}$) FWHM depending on the electron temperature. Unfortunately, this relationship is very difficult to establish on the basis of the experimental data because FWHM is susceptible to ion broadening. As is apparent from the BG theory, this effect affects FWHM by the ion broadening parameter $A \sim n_e^{1/4}$ and the Debye shielding parameter $r \sim n_e^{1/6}$.

Another parameter describing the line profile is the asymmetry defined here as the ratio of the half widths at half

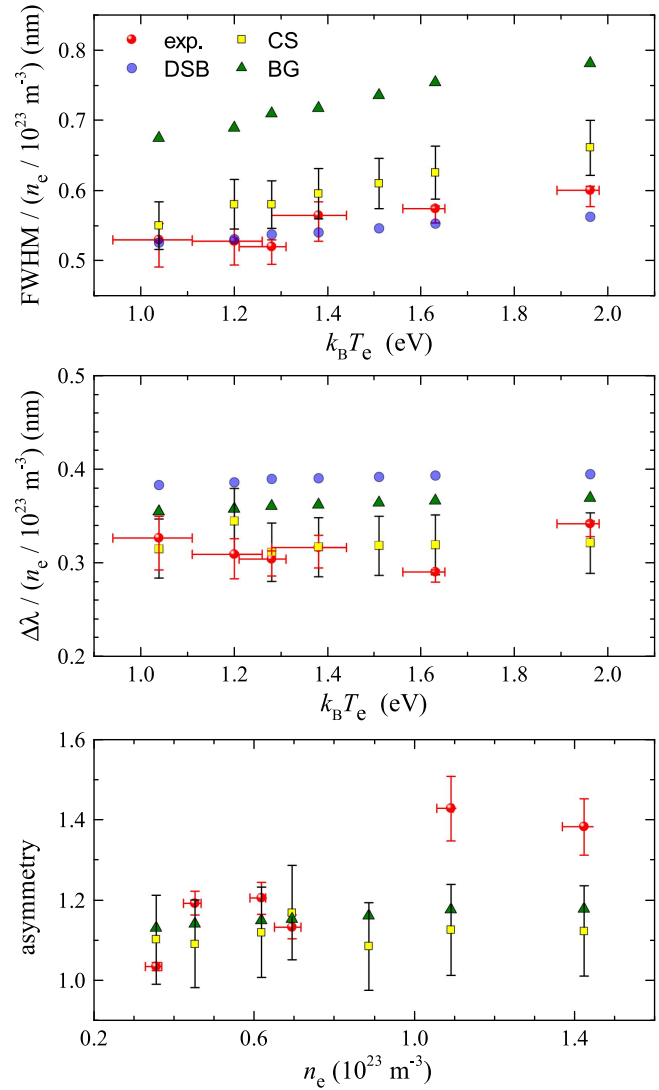


Figure 11. FWHM of the isolated Li I 497 nm line normalized to n_e , its shift $\Delta\lambda$ and asymmetry defined as $\text{HWHM}_{\text{red}}/\text{HWHM}_{\text{blue}}$. BG and DSB—calculations made by Benett and Griem [1, 12] and by Dimitrijević and Sahal-Bréchet [13–15], respectively.

maximum of its red and blue parts. The asymmetry of the line profile is mainly the effect of the ions. Reasonable agreement between calculations (CS and BG) and the experiment has been found for electron densities lower than 10^{23} m^{-3} . For higher densities, the asymmetry of the experimental profiles is about twice as large as of calculated ones. This latter discrepancy may be due to inhomogeneous plasma volume under study. The smaller the plasma plume the larger inhomogeneities, which occurs for shorter delays. Other sources of this discrepancy may also be hydrodynamic processes in the plasma like retro-reflected shock waves, particularly significant in the early stages of its evolution.

6. Summary and conclusions

In this work we report the results of the theoretical and experimental studies of Stark profiles of the Li I 460 nm with

forbidden components and of the isolated 497 nm one. In the experiment, plasma was induced from the alumina pellet, with some content of Li_2CO_3 , irradiated by a nanosecond Nd:YAG laser radiation at 1064 nm. Spatially- and temporally-resolved plasma diagnostics was performed by the use of the laser TS technique, independently of plasma emission spectra and free from assumptions about the plasma equilibrium state and its composition. The spatially resolved plasma spectra with Li lines of interest were obtained from the measured, laterally integrated spectra applying the inverse Abel transform. In further investigations only the results for the plasma axis were considered.

The Stark profiles were calculated by CS method. Calculations were performed for TS-inferred electron densities and temperatures, in the range from $1.422 \times 10^{23} \text{ m}^{-3}$ to $3.55 \times 10^{22} \text{ m}^{-3}$ and from 1.96 eV to 1.04 eV, respectively. Unlike the earlier calculations presented in [18], the Hamiltonian of the radiator system contained all states with n from 2 to 5, inclusive and not only the closest to the transition states with $n = 2$ and 4. Such improvements were required to achieve high accuracy matching that of the present measurements.

Our studies show very good agreement between experimental Stark profiles and those calculated using CS method. Their parameters—widths and shifts—agree within the uncertainty limits of less than 10%. Also, it should be clearly stated that, from plasma diagnostic point of view, the 460 nm line is a much better n_e probe than any isolated line due to its distinct spectroscopic Stark signature with two peaks and much larger width.

Further advances in the study of Stark profiles emitted from LIP will need lifting the assumption of isothermal plasma. This in turn requires the development of independent plasma diagnostic methods that determine not only the electron density and temperature, but also the plasma composition and the temperature of heavy particles.

Acknowledgments

We are grateful to S Sahal-Bréchet and MS Dimitrijević for fruitful discussions. MG wishes to acknowledge the partial support from the Ministry of Education, Science and Technological Development of Republic Serbia under Project no. 171014. The work of ES was supported in part by the Israel Science Foundation. The research was carried out with the equipment purchased thanks to the financial support of the European Regional Development Fund in the framework of the Polish Innovation Economy Operational Program (Contract No. POIG.02.01.00-12-023/08).

ORCID iDs

Krzysztof Dzierżęga  <https://orcid.org/0000-0002-6708-7775>

References

- [1] Griem H R 1974 *Spectral Line Broadening by Plasmas* (New York: Academic)
- [2] Konjević N, Ivković M and Sakan N 2012 *Spectrochim. Acta B* **76** 16
- [3] Konjević N 2001 *Plasma Sources Sci. Technol.* **10** 356
- [4] Ivković M, González M, Jovičević S, Gigosos M and Konjević N 2010 *Spectrochim. Acta B* **65** 234
- [5] González M Á, Ivković M, Gigosos M A, Jovičević S, Lara N and Konjević N 2011 *J. Phys. D: Appl. Phys.* **44** 194010
- [6] Ivković M, González M, Lara N, Gigosos M and Konjević N 2013 *J. Quant. Spectrosc. Radiat. Transfer* **127** 82
- [7] Gigosos M A and González M Á 2009 *Astron. Astrophys.* **503** 293
- [8] Lara N, González M Á and Gigosos M A 2012 *Astron. Astrophys.* **542** A75
- [9] Kramida A, Ralchenko Y, Reader J and NIST ASD Team 2016 NIST Atomic Spectra Database (version 5.4)
- [10] Konjević N and Roberts J R 1976 *J. Phys. Chem. Ref. Data* **5** 209
- [11] Lesage A 2009 *New Astron. Rev.* **52** 471
- [12] Benett S and Griem H 1971 *Technical Report* 71-097 University of Maryland, College Park, Maryland
- [13] Dimitrijević M S and Sahal-Bréchet S 1991 *J. Quant. Spectrosc. Radiat. Transfer* **46** 41
- [14] Dimitrijević M S and Sahal-Bréchet S 1991 *Bull. Obs. Astron. Belgr.* **143** 29
- [15] Sahal-Bréchet S, Dimitrijević M S and Morecbau N 2017 Stark-B database for Stark broadening of isolated lines of atoms and ions in the impact approximation. <http://stark-b.obspm.fr>
- [16] Grechikhin L I and Tyunina E S 1963 *Tepl. Vysokih Temp.* **1** 399
- [17] Sassi M 1972 *J. Quant. Spectrosc. Radiat. Transfer* **12** 75
- [18] Cvejić M, Stambulchik E, Gavrilović M R, Jovičević S and Konjević N 2014 *Spectrochim. Acta B* **100** 86
- [19] Dzierżęga K, Mendys A, Pokrzywka B, Zawadzki W and Pellerin S 2014 *Spectrochim. Acta B* **98** 76
- [20] Stambulchik E and Maron Y 2006 *J. Quant. Spectrosc. Radiat. Transfer* **99** 730
- [21] Cvejić M, Gavrilović M, Jovičević S and Konjević N 2013 *Spectrochim. Acta B* **85** 20
- [22] Evans O E and Katzenstein J 1969 *Rep. Prog. Phys.* **32** 207
- [23] Drawin H W 1963 *Z. Phys.* **172** 181
- [24] Stambulchik E and Maron Y 2010 *High Energy Density Phys.* **6** 9
- [25] Stamm R and Voslamber D 1979 *J. Quant. Spectrosc. Radiat. Transfer* **22** 599
- [26] Gigosos M A 2014 *J. Phys. D: Appl. Phys.* **47** 343001
- [27] Verlet L 1967 *Phys. Rev.* **159** 98
- [28] Stambulchik E, Fisher D V, Maron Y, Griem H R and Alexiou S 2007 *High Energy Density Phys.* **3** 272
- [29] Ferri S et al 2014 *Atoms* **2** 299
- [30] Baranger M 1958 *Phys. Rev.* **112** 855
- [31] Stambulchik E and Maron Y 1997 *Phys. Rev. A* **56** 2713
- [32] Tsigutkin K, Stambulchik E, Maron Y and Tauschwitz A 2005 *Phys. Scr.* **71** 502
- [33] Cowan R D 1981 *The Theory of Atomic Structure and Spectra* (Berkeley, Los Angeles, London: University of California Press)
- [34] Gomez T A, Nagayama T, Kilcrease D P, Montgomery M H and Winget D E 2016 *Phys. Rev. A* **94** 022501
- [35] Stambulchik E, Alexiou S, Griem H R and Kepple P C 2007 *Phys. Rev. E* **75** 016401
- [36] Bardet J P and Valognes J C 1983 *J. Phys.* **44** 797

- [37] Mendys A, Kanski M, Farah-Sougueh A, Pellerin S, Pokrzywka B and Dzierżęga K 2014 *Spectrochim. Acta B* **96** 61
- [38] Cvejić M, Dzierżęga K and Pięta T 2015 *Appl. Phys. Lett.* **107** 024102